Biosensors and Bioelectronics 142 (2019) 111538

Contents lists available at ScienceDirect

Biosensors and Bioelectronics

journal homepage: www.elsevier.com/locate/bios

Electrochemical monitoring of the impact of polymicrobial infections on *Pseudomonas aeruginosa* and growth dependent medium

Olja Simoska[a], Marta Sans[a], Livia S. Eberlin[a], Jason B. Shear[a], Keith J. Stevenson[b,*]

[a] Department of Chemistry, University of Texas at Austin, 1 University Station, Stop A5300, Austin, TX, 78712, USA
[b] Center for Energy Science and Technology, Skolkovo Institute of Science and Technology, Bolshoi Boulevard 30 Bld. 1, Moscow, 121205, Russia

ARTICLE INFO

Keywords:
Pseudomonas aeruginosa
Bioelectroanalytical sensors
Phenazine metabolites
Polymicrobial communities
Pathogenic infections
Real-time electrochemical monitoring
Carbon ultramicroelectrode arrays

ABSTRACT

The opportunistic human pathogen *Pseudomonas aeruginosa* (*Pa*) causes several infections acquired in a healthcare setting. During initial stages of infection, *Pa* produces redox-active phenazine metabolites, including pyocyanin (PYO), 5-methylphenazine-1-carboxylic acid (5-MCA), and 1-hydroxyphenazine (OHPHZ), which have toxic effects on surrounding host cells and/or other microbes. Rapid and sensitive detection of these metabolites provides important evidence about the onset of *Pa* infections. Herein, we investigate differences in *Pa* phenazine production and dynamics in polymicrobial communities. Specifically, *Pa* was co-cultured with two pathogens of clinical relevance, *Staphylococcus aureus* (*Sa*) and *Escherichia coli* (*Ec*), which typically populate infection sites with *Pa*. Phenazine production rates and biosynthesis dynamics were electrochemically monitored during a 48-h period using recently developed transparent carbon ultramicroelectrode arrays (T-CUAs). Moreover, the effect on phenazine production rates and dynamics was explored in two growth media, lysogeny broth (LB) and tryptic soy broth (TSB). The concentrations of PYO and highly reactive 5-MCA were determined in different polymicrobial culture samples in both media. The results demonstrate that other bacterial pathogens noticeably influence *Pa* phenazine production and dynamics. In particular, *Sa* caused a decrease in phenazine production in TSB. However, the presence of *Ec* in polymicrobial samples drastically inhibited phenazine production rates in both LB and TSB. Conclusively, the media type significantly influences phenazine product distribution, especially in polymicrobial co-cultures, signifying the need for analytical standardization of simulation media in the study of polymicrobial communities.

1. Introduction

The development of severe microbial infections remains a challenge (Boucher et al., 2009; Klevens et al., 2007) in healthcare facilities as immune-compromised hosts are exposed to communities of pathogenic bacteria (Bassler and Losick, 2006; Henke and Bassler, 2004; Stevens et al., 2012). Prompt detection, identification and real-time monitoring of early stages of infectious diseases, such as pneumonia, invasive wounds, and bloodstream infections (Bowler et al., 2001; Magill et al., 2014), are essential in disease prevention and determining effective treatment strategies. Typically, these hospital-contracted infections are populated by multiple microbial species, including *Pseudomonas aeruginosa* (*Pa*), *Staphylococcus aureus* (*Sa*), *Escherichia coli* (*Ec*), *Enterococcus faecalis*, and *Staphylococcus epidermidis* (Bertesteanu et al., 2014; Giacometti et al., 2000). Current hospital diagnosis methods involve use of cell-culturing platforms, which classify specimens based on growth patterns observed in different media with selective growth components and/or antibiotics. These approaches, however, often require several days before pathogen identity is known, resulting in an increased antibiotic resistance as patients undergo treatments with broad-spectrum antibiotics (Llor and Bjerrum, 2014). As an alternative to the standard techniques, various electrochemical sensor platforms have been developed, which offer rapid identification, direct detection, and quantification of pathogenic signaling metabolites and byproducts.

In previous studies, our group has reported an inexpensive, facile and adaptable electrochemical platform using transparent carbon ultramicroelectrode arrays (T-CUAs) (Duay et al., 2015, 2014). These sensors provide advantages in contrast to other electrochemical sensing devices, including amplified current responses, fast response times, large linear dynamic ranges (LDRs), high signal-to-noise (S/N) ratios and lower limits of detection (LODs) (Duay et al., 2015, 2014; Elliott et al., 2017a, 2017b; Simoska et al., 2019). As their electroactive material is comparable to glassy carbon, T-CUAs are inert, highly conductive and extremely biocompatible. This electroanalytical platform

* Corresponding author.
E-mail address: K.Stevenson@skoltech.ru (K.J. Stevenson).

https://doi.org/10.1016/j.bios.2019.111538
Received 19 June 2019; Received in revised form 16 July 2019; Accepted 24 July 2019
Available online 25 July 2019

has been used to rapidly detect the common opportunistic human pathogen *Pa* (Elliott et al., 2017b; Simoska et al., 2019). Similar to other pathogens, *Pa* readily establishes infections in hosts with compromised immune systems and in those suffering from conditions, such as chronic wounds, lung infections, and severe burns (Fetzer et al., 1967; Fick, 1989; Ringen and Drake, 1952; Walker, 2004). Using electrochemical sensors, *Pa* can be easily detected via the production of redox-active pyocyanin (PYO) (Alatraktchi et al., 2016a, 2016b; Elliott et al., 2017b; Jayaseelan et al., 2013; Simoska et al., 2019; Webster et al., 2014), which is a bacterial warfare toxin secreted as a secondary metabolite (Jayaseelan et al., 2013). Because it is produced uniquely by *Pa* during early infection stages (Mavrodi et al., 2010), PYO is considered a useful electroactive biomarker indicative of infections caused by this pathogen (Dietrich et al., 2006).

Although a significant amount of research has focused on developing electrochemical platforms for the detection of PYO (Alatraktchi et al., 2016a, 2016b; 2018; Elliott et al., 2017b; Sharp et al., 2010; Webster and Goluch, 2012), this is only the end product of *Pa* phenazine biosynthetic pathway (Mavrodi et al., 2010, 2006; L. S. Pierson and E. A. Pierson, 2010). PYO is synthesized through a cascade of complex metabolic reactions involving various genes. In addition to PYO, *Pa* produces several phenazine derivatives in this biosynthetic route, including a side product, 1-hydroxyphenazine (OHPHZ), and a short-lived, reactive precursor, 5-methylphenazine-1-carboxylic acid (5-MCA) (Mavrodi et al., 2006). Phenazines are small, redox-active, nitrogen-containing heterocyclic molecules, which engage in reduction and oxidation processes in the presence of molecular oxygen. Thus, they play key roles in altering metabolism, modify immune responses and damage host tissue (Glasser et al., 2014; Hendiani et al., 2019; Mavrodi et al., 2006; L. S. Pierson and E. A. Pierson, 2010). Additionally, a recent study reported that phenazines interact with antibiotics, thus influencing treatment of *Pa* infections (Schiessl et al., 2019). Detection and examination of their relative quantities produced during various growth stages could provide a better understanding of phenazine functions in *Pa* virulence mechanisms.

In a recent study, we have demonstrated use of T-CUAs for the real-time monitoring of phenazine production and metabolism dynamics from *Pa* cell cultures in simulated growth media (Simoska et al., 2019). Our previous work increased knowledge about phenazine biosynthesis in *Pa* monocultures, yet a follow-on study is necessary to understand the impact of polymicrobial cultures on phenazine production and dynamics, in particular when *Pa* is cultured alongside other bacterial pathogens in the same growth environments. Microorganisms seldom live in isolation as in almost all environments, multiple bacterial species inhabit diverse microbial communities in which interactions between species shape biological activities of cellular populations (Atkinson and Williams, 2009; J.-H. Lee and J. Lee, 2010; Mirani et al., 2018; O'Brien and Fothergill, 2017). During polymicrobial infections, cellular communication within complex cellular communities can alter virulence and/or host responses (Bertesteanu et al., 2014; Korgaonkar et al., 2013; J.-H. Lee and J. Lee, 2010). As a prominent pathogen in polymicrobial infections, *Pa* often displays either synergistic or adversarial relationships with other bacteria, thus increasing disease severity (Bergeron et al., 2017). Therefore, *Pa* phenazine production and biosynthesis dynamics in polymicrobial environments need to be examined, as they represent a clinically relevant problem. Although various fluorescence microscopy-based methods have been employed (Connell et al., 2013; Korgaonkar et al., 2013; Sullivan et al., 2011), additional analytical tools are necessary to quantitatively study the dynamic microbe-microbe interactions, in real time (Bergeron et al., 2017; Goluch, 2017; D.-H. Lee et al., 2013).

Herein, we demonstrate use of T-CUAs for the quantitative, real-time electrochemical monitoring of the impact of polymicrobial communities on *Pa* phenazine production where *Pa* is co-cultured with other clinical pathogens, *Sa* and *Ec*, in two different growth media that are predominately used for such bacterial-based cell culture studies. Our results, during 48 h bacterial growth, show distinct differences in amounts of phenazine products and intermediates secreted by *Pa* in mono- and polymicrobial communities. Specifically, when *Pa* was co-cultured with *Ec*, the concentrations of cellular PYO were significantly reduced compared to amounts produced in monoculture samples, in both media. Yet when *Pa* was cultured alongside *Sa*, PYO concentrations were lower in only one media. These results show that the amounts of phenazine derivatives produced during growth depend on both various environmental factors in the media and presence of other microbes. These electrochemical results were confirmed by desorption electrospray ionization mass spectrometry (DESI-MS) imaging studies to determine differences in relative abundances of key growth media components and nutrients, and to identify other cellular metabolites produced in polymicrobial cultures.

2. Experimental methods

All procedural information is given in the supplementary information (SI).

3. Results and discussion

3.1. Pa phenazine biosynthetic pathway in polymicrobial environments

During stationary phase, *Pa* strains actively produce phenazines, including phenazine-1-carboxylic acid (PCA), OHPHZ, 5-MCA, and PYO (Mavrodi et al., 2001), which are biomolecules with key functions in microbial virulence (Bosire and Rosenbaum, 2017; Diederich et al., 2017). Due to their small sizes and minor structural variations (Sullivan et al., 2011), these highly diffusible species are extremely challenging to study and identify as they undergo redox changes (Dietrich et al., 2006). The influence of polymicrobial communities on *Pa* phenazine production remains unclear (Mavrodi et al., 2001), thus research addressing distinct quantities and ratios of phenazine products and intermediates is necessary to understand interactions of *Pa* with other co-infecting species (here, *Sa* and *Ec*) (L. S. Pierson and E. A. Pierson, 2010). Phenazines are derived from shikimic acid pathways, where PYO production begins with the conversion of chorismic acid to PCA. Enzyme PhzM then converts PCA is converted to highly reactive 5-MCA. In the final step, monooxygenase PhzS converts 5-MCA to PYO (Parsons et al., 2007).

3.2. Phenazines and interferents in polymicrobial cultures

A general concern with the use of electrode-based sensors for biological applications is the device selectivity, particularly the ability of the working electrode to distinguish phenazine targets from potential interferents. As they grow in distinct multi-species environments, pathogens produce a variety of redox-active, small molecules as secondary metabolites (Zheng et al., 2015). In this specific application, species secreted by other bacteria could potentially interfere with T-CUA responses in the potential window where redox peaks of *Pa* phenazines are observed. To test potential interferences, the two bacterial pathogens used in this study, *Sa* and *Ec*, were electrochemically examined after 24 h of cell growth in lysogeny broth (LB) and tryptic soy broth (TSB). The square wave voltammograms (SWVs) in Fig. 1 demonstrate that the distinguishable electroactive peaks are due to *Pa* phenazine species only. Specifically, redox-active metabolites, PYO, 5-MCA, and OHPHZ are produced by *Pa* in LB and TSB media at 24 h. The identities of these metabolites were confirmed using mass spectrometry methods in our previous study (Simoska et al., 2019). The SWVs for *Sa* and *Ec* display nearly identical current responses compared to background currents (LB or TSB). These results confirm that *Sa* and *Ec* do not produce electrochemically active species in the potential window (-0.7 to 0.0 V vs SCE) used. Furthermore, current responses for *Sa* and *Ec* co-cultures in TSB and LB were also recorded at 24 h growth, which

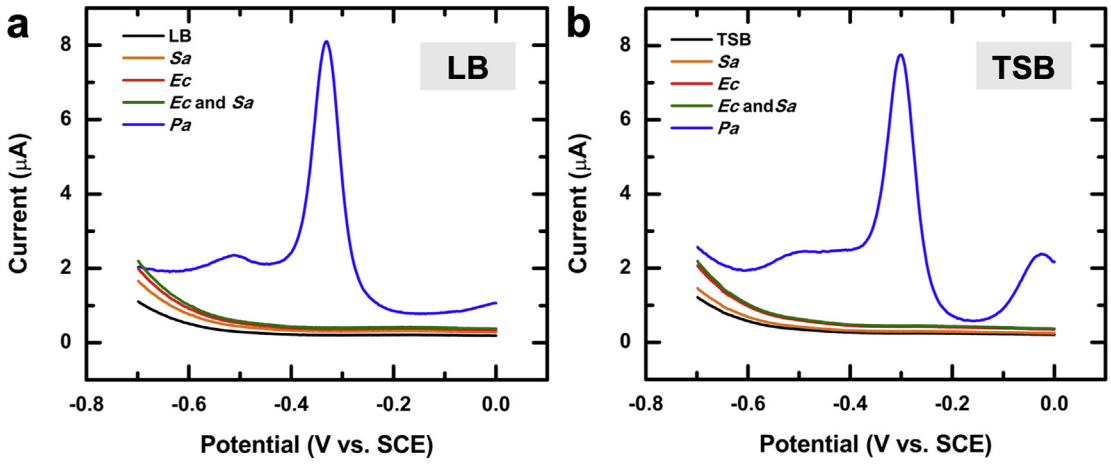

Fig. 1. Square wave voltammograms of bacterial cultures at 24 h of growth in (a) LB and (b) TSB. The redox peaks around −0.256 V vs. SCE result from PYO present in *Pa* liquid-batch cultures. No interfering redox active peaks are observed from *Sa* and *Ec* cultures in the working potential window.

demonstrate that the interaction between *Sa* and *Ec* does not produce redox-active metabolites in the potential window used here. In addition to the presence of other pathogens, several growth media components (e.g., glucose, gluconic acid, uric acid, ascorbic acid, NADH, NADPH, NAD, NADP, H_2O_2) could have interference effects, impacting electrode responses. Previous research has shown that biologically relevant concentration of these common biological interferents have redox signatures at more positive potentials, which are outside of the potential widow in this study (Alatraktchi et al., 2016b; Simoska et al., 2019). Among phenazine metabolites, *Pa* secretes various other biological metabolites, including non-electrochemically active N-Acyl homoserine lactones, as well as electrochemically active species such as pyoverdine, 2-heptyl-3-hydroxy-4-quinolone (PQS) and its immediate precursor, 2-heptyl-4-hydroxyquinoline (HHQ). Previous research has shown that pyoverdine, PQS and HHQ have electrochemical signatures at more positive potentials, which fall outside of the potential window used herein (Buzid et al., 2016; Gandouzi et al., 2019). Therefore, the redox peaks observed in Fig. 1 are due to *Pa* phenazine metabolites, which were identified with mass spectrometry methods in our recent study (Simoska et al., 2019). Thus, using an electrochemical potential window specific to *Pa* phenazines, their production rates in polymicrobial samples were monitored on T-CUAs, in real time.

3.3. Real-time electrochemical detection and quantification of Pa phenazines in polymicrobial cultures

Real-time, continual electrochemical monitoring, over 48 h, was performed to study the effect of polymicrobial communities' dynamics on phenazine production in two different media. Combinations of *Pa* co-cultured together with (1) *Sa*, (2) *Ec* or (3) both *Sa* and *Ec*, were prepared in either LB or TSB media to examine how other bacteria impact phenazine biosynthesis production in polymicrobial cultures. To start cell growth, individually grown liquid-batch cultures of *Pa*, *Sa* and *Ec* were diluted into fresh media to achieve identical initial optical densities. Polymicrobial samples were incubated at 37 °C and shaken at 150 rpm for a 48-h period, during which optical density (absorbance at 600 nm) measurements were performed to monitor growth stages in LB and TSB. Fig. 2 shows fairly sigmoidal growth curves for mono- and poly-microbial samples in LB and TSB. The initial 4 h (0–3 h) represent the exponential phase, after which bacteria enter the stationary stage, as indicated by the resulting plateau in the growth curves. During the stationary phase, population size remains the same since the rate of cell growth equals the rate of cell death. When grown individually, *Pa* cells initially show higher optical densities in LB media than TSB, however, after 12 h, optical measurements are higher in TSB relative to LB. When *Pa* was co-cultured with *Sa* in LB, the time-dependent optical densities are marginally higher compared to *Pa* monoculture sample (Fig. 2a), indicating the presence of another bacterial species. Similarly, the polymicrobial combination samples with *Ec* in LB show optical densities higher than those for *Pa* only and *Sa* sample. These higher doubling rates in combination samples containing *Ec* are likely a result of *Ec* growing faster than *Sa* and *Pa* (D.-H. Lee et al., 2013). On the other hand, all three polymicrobial combinations in TSB display higher optical densities than the control *Pa* monoculture at nearly all time points. These results suggest that media also has an effect on bacterial growth rates as some bacteria might outgrow others in competing for resources and nutrients (Rohmer et al., 2011). Although these optical density measurements show differences between mono- and poly-microbial samples in two media, this method provides no information about quantities of phenazine metabolites produced during different growth stages.

Therefore, in tandem with optical density, electrochemical measurements, using SWV, were performed in a time-based fashion to simultaneously detect various phenazines, including PYO, 5-MCA, OHPHZ, and an unknown derivative, in polymicrobial environments (Fig. 3). Specifically, phenazine production was monitored directly from different polymicrobial samples every hour during the initial 12 h, followed by every 3 h until 24 h, then every 6 h till 48 h. To quantify concentrations of cellular metabolites in polymicrobial samples in LB and TSB, the data were analyzed using background current subtraction and previously constructed calibration curves (Simoska et al., 2019). In this study, real-time electrochemical measurements of cellular PYO and 5-MCA in polymicrobial cell cultures were performed six times in each media to validate high reproducibility. Thus, error bars (Fig. 4) represent the standard deviation between the six replicates. Fig. 3 shows the resulting SWVs for different cell combination samples in LB and TSB, where the current-potential responses are plotted as a function of time. In previous research, mass spectrometry methods, including DESI-MS and nano-electrospray ionization (nano-ESI), were used to confirm the identities of phenazine metabolites observed in our electrochemical data (Simoska et al., 2019). Specifically, cellular PYO has a redox-active peak at −0.256 V vs SCE while highly reactive 5-MCA shows its electrochemical fingerprint at −0.115 V vs SCE (Fig. 3). Additionally, the shoulder peak observed at a more negative potential (−0.512 V vs SCE) after 21 h, is corroborated by OHPHZ, a degradation, side product of PYO (Simoska et al., 2019; Sismaet et al., 2017). Finally, in certain samples, an unknown species is detected at a more positive potential of −0.0112 V vs SCE at later stages of growth. Unfortunately, the identity of this species remains elusive, but it is suspected to be a highly unstable 5-MCA derivative or a degradation species. Presently, this

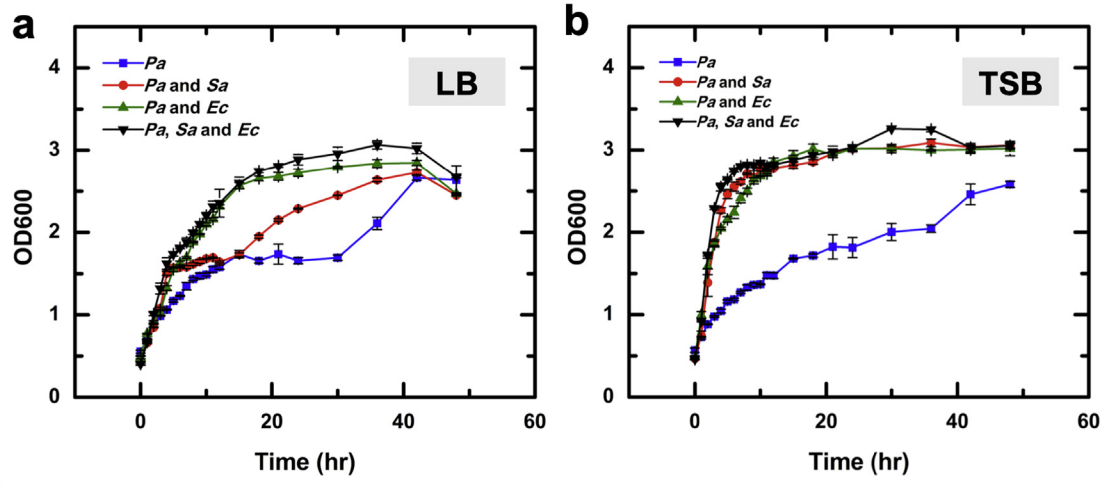

Fig. 2. Optical density measurements at 600 nm (OD600) of polymicrobial co-cultures determined at various time points of growth in (a) LB and (b) TSB broth. Error bars represent the standard deviation between six samples.

metabolite can only be detected using our electrochemical T-CUA platform, however, MS methods need optimization to enable its identification. The marginal shifts in PYO redox peaks in SWVs (Fig. 3) are due to increasing pH values in liquid-batch cultures in the two media (Shah et al., 2013; Simoska et al., 2019).

The SWV responses in Fig. 3 show the temporal changes in phenazine dynamics in the different microbial samples in LB and TSB. When *Pa* is individually cultured, concentrations of cellular PYO do not change significantly in both broths during the exponential growth phase (0–3 h). Initially, PYO concentrations in LB are approximately two times higher compared to those in TSB for *Pa* cultures. In the stationary phase, *Pa* cells produce increasing amounts of PYO until 21 h, after which PYO concentrations decrease and plateau in LB and TSB as observed in the resulting current responses. While PYO levels do not significantly differ between LB and TSB during 4–12 h, PYO amounts in TSB are 1.3 times higher than in LB broth after 15 h (Fig. 3a and b, Tables S1–S2). During 21 h growth, increasing PYO production rates correlate to increased intercellular communication (Schiessl et al., 2019; Simoska et al., 2019). Extended growth in the stationary stage results in a decrease in production of virulence factors. The time-dependent SWVs show different current responses when additional pathogens are cultured with *Pa* in LB and TSB. When co-cultured with *Sa* in LB, *Pa* produces PYO amounts that are twice lower than those in *Pa* sample during 0–12 h. After 15 h, levels of cellular PYO in *Pa* and *Sa* combination sample in LB are similar to those in *Pa* alone (Fig. 3b). On the other hand, when grown with *Ec*, *Pa* produces PYO concentrations that are two times lower compared to *Pa* only, at all time points of growth (Fig. 3c). For samples comprised of all three microorganisms in LB, PYO concentrations are approximately five-fold lower, on average, relative to individual *Pa* culture (Fig. 3d). These results, summarized in Fig. 4a, show the determined PYO concentrations as a function of growth time in polymicrobial samples in LB. Similarly to LB, the presence of *Sa* and *Ec* changes phenazine production rates in TSB. PYO concentrations decrease nearly four times when *Pa* is co-cultured with *Sa* in TBS (Fig. 3f). The presence of *Ec* in TBS significantly reduces phenazine production (Fig. 3g and h) resulting in notably smaller quantities of PYO. These quantitative results, summarized in Fig. 4b, illustrate PYO concentrations at different time points of growth for polymicrobial combinations in TSB. The concentrations of PYO produced by *Pa* in polymicrobial samples in LB and TSB are outlined in Tables S1–S2 in the supplementary information. For individual *Pa* cultures, the maximum PYO concentrations were determined to be 150 ± 1 μM and 190 ± 5 μM in LB and TSB, respectively, at 21 h. For polymicrobial samples in LB, *Pa* produces maximum PYO concentrations of 150 ± 1 μM in *Pa* and *Sa*, 72 ± 1 μM in *Pa* and *Ec*, and 28 ± 1 μM in *Pa*, *Sa* and *Ec* sample at 21 h growth. When cultured together with *Sa* in TSB, *Pa* produces 78 ± 2 μM as the highest PYO concentration (at 21 h). The maximum concentration of PYO for *Pa* and *Ec* sample in TSB was 9.3 ± 0.2 μM at 21 h. At 48 h, *Pa* produced a maximum PYO concentration of 8.2 ± 0.5 μM in the polymicrobial combination comprising all three pathogens in TSB.

These results demonstrate that in addition to other bacterial pathogens, the media composition largely impacts phenazine production rates. Briefly, the presence of *Sa* does not have a large effect on *Pa* phenazine production in LB (Fig. 4a). The ability of PYO to inhibit *Sa* growth has been reported (Noto et al., 2017), which might result in preferential growth of *Pa*. A previous study has shown that *Sa* promotes growth and increased aggregation of *Pa*, thus suggesting that these two pathogens can co-exist and interact in a beneficial manner (Alves et al., 2018). Additionally, research has demonstrated *Pa* to be the dominant growing species when co-cultured with *Sa* (Mirani et al., 2018). These reports on microbial interactions potentially explain why PYO concentrations are marginally higher when *Pa* is grown with *Sa* in LB. However, this is not observed for *Pa* and *Sa* sample in TSB, suggesting the phenazine production rates greatly depend on media composition. When *Pa* is co-cultured together with *Sa* in TSB, a decrease in PYO concentrations of approximately 60% is observed (Fig. 4b). Unlike in LB, *Pa* and *Sa* likely engage in competitive behaviors for various nutrients in TSB. The presence of *Ec* influences phenazine production in both media. Specifically, PYO amounts are approximately 50% lower in *Pa* and *Ec* sample compared to *Pa* sample in LB (Fig. 4a). Furthermore, *Ec* considerably slows down phenazine production in TSB, as noted by approximately 95% lower PYO concentrations compared to amounts produced in *Pa* monocultures (Fig. 4b). A previous study has shown *Ec* to not only dominate co-cultures but also hinder *Pa* growth in both nutrient-limited and enriched conditions (Culotti and Packman, 2014), resulting in smaller amounts of *Pa* cells compared to monocultures. Additionally, research has shown *Ec* to dominate multi-species environments, in particular, when co-cultured with either *Pa* or *Sa* (Mirani et al., 2018), suggesting that *Ec* consumes nutrients at a fast pace. In addition, *Ec* might produce unique cellular signaling molecules that can directly impact *Pa* phenazine production, which is discussed in subsequent discussion sections.

Previously, Santiveri and co-workers studied PYO production in various polymicrobial cultures in different media using another electrochemical approach (Santiveri et al., 2018). Their reported results showed that the presence of additional pathogens in growth media did not affect the relative rates of PYO produced by *Pa* (Santiveri et al.,

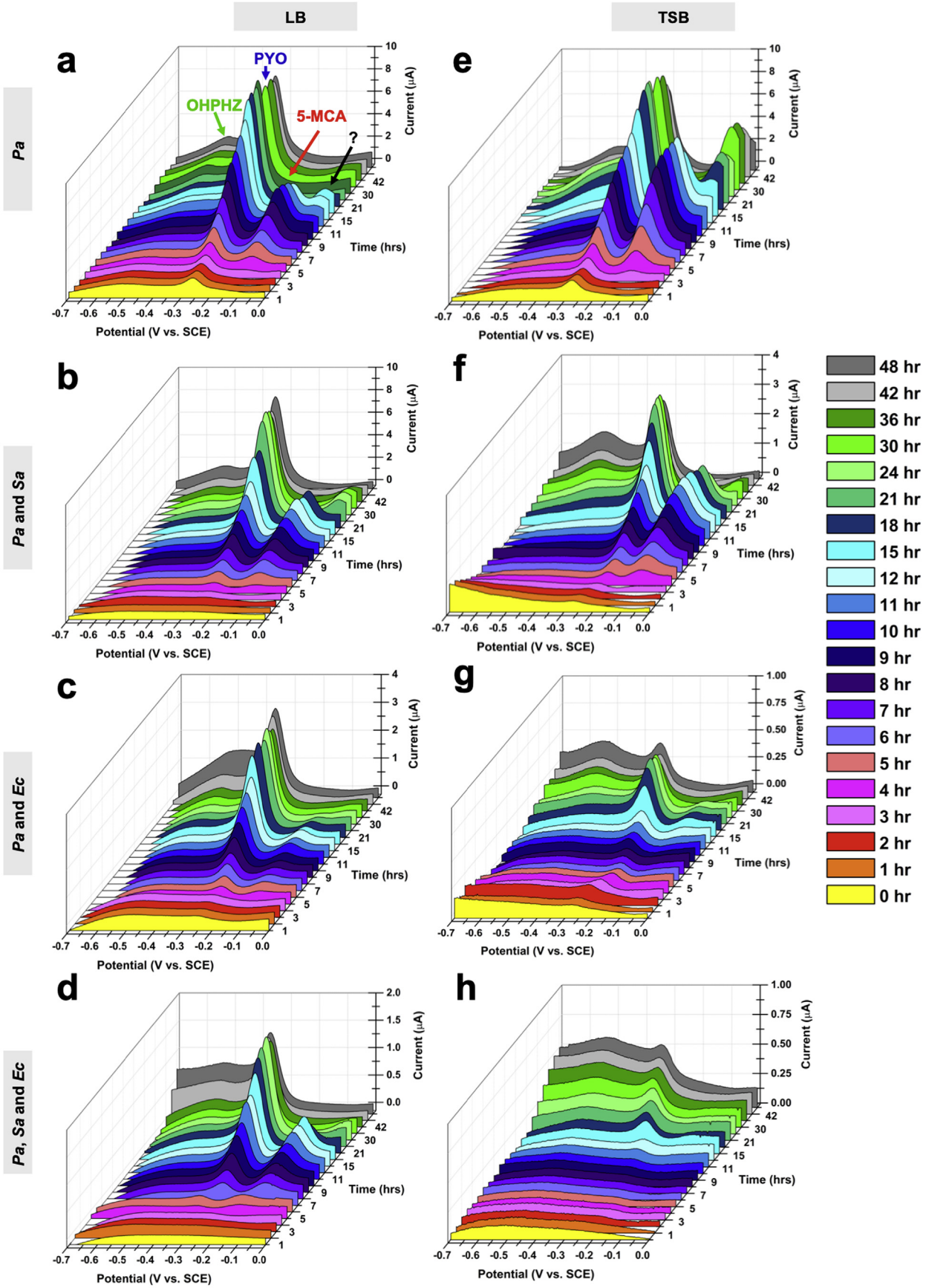

Fig. 3. Time-dependent square wave voltammograms recorded for 0–48 h for (a) *Pa*, (b) *Pa* and *Sa*, (c) *Pa* and *Ec*, and (d) *Pa*, *Sa* and *Ec* in LB media, and (e) *Pa*, (f) *Pa* and *Sa*, (g) *Pa* and *Ec*, and (h) *Pa*, *Sa* and *Ec* in TSB media. The redox peak at −0.256 V vs. SCE corresponds to PYO, while the emerging peak at a more positive potential (−0.115 V vs. SCE) is due to 5-MCA. The identity of electroactive peaks at a more positive potential than 5-MCA observed in some bacterial cultures remains elusive, however, it might be a reactive derivative species of 5-MCA. Shoulder peak observed at −0.5 V vs. SCE are related to PYO side product, 1-

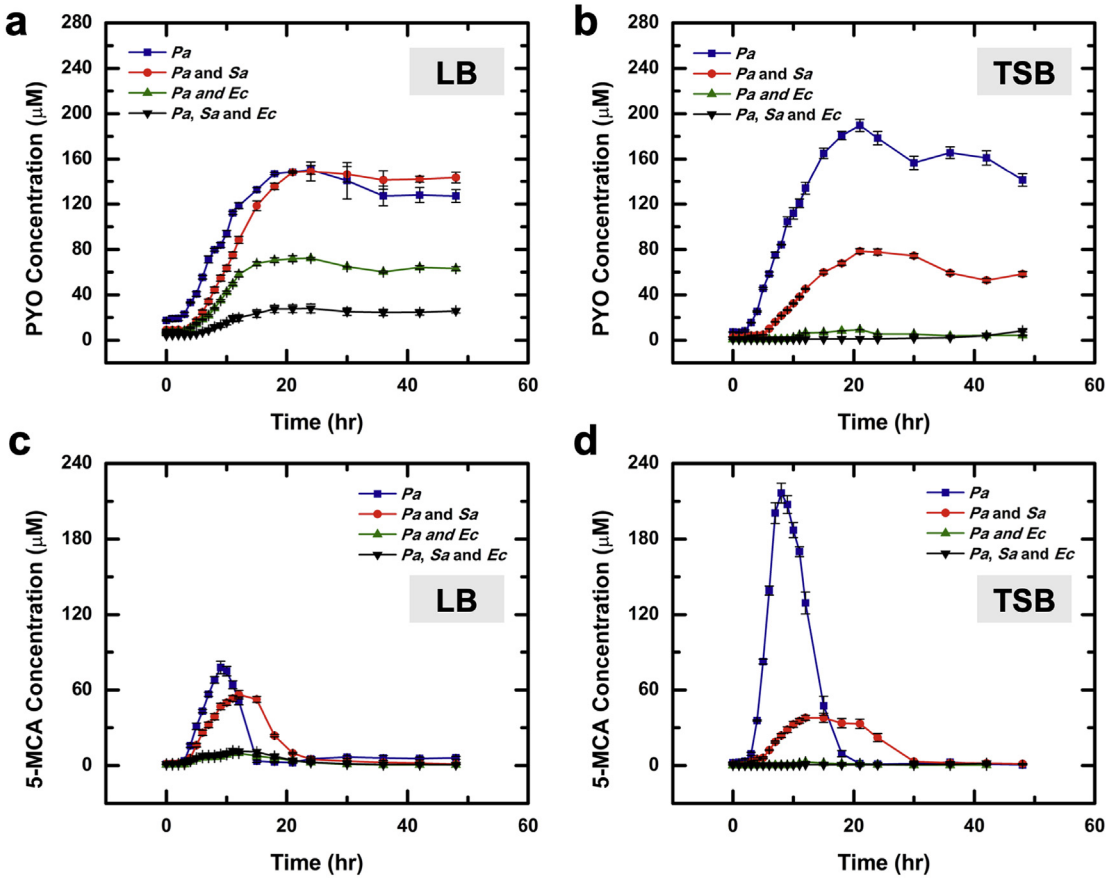

Fig. 4. PYO concentrations determined from *Pa* in different microbial co-cultures in (a) LB and (b) TSB growth media, as a function of time. 5-MCA concentrations secreted from *Pa* in (c) LB and (d) TSB media, were determined from 5-MCA/PYO current peak ratios, relating to phenazine kinetics. Error bars show the standard deviation between six samples. PYO and 5-MCA concentrations are outlined in Tables S1–S4.

2018), which contradicts our evidence. In their study, to detect and quantify PYO concentrations, researchers used a carbon, macro-size working electrode (3 mm diameter), which might not have the sensitivity, large linear dynamic ranges, and rapid response times necessary to appropriately distinguish differences in production rates not only for PYO, but also for intermediate species in polymicrobial environments. In contrast to their electrochemical platform, requiring the use of a fresh electrode for each new time-based measurement, we have shown that T-CUAs are continually used for measurements for the entire duration of 48-h experiments (Simoska et al., 2019).

3.4. Dynamics of phenazine production in polymicrobial environments

Along with electrochemical quantification of PYO concentrations in polymicrobial co-cultures, dynamics of the phenazine biosynthetic pathway was monitored. The current-potential responses in Fig. 3 display remarkable distinctions in production rates of 5-MCA in polymicrobial samples in LB and TSB. These data demonstrate dissimilarities in dynamics of phenazine biosynthesis processes, suggesting a dependence on environmental factors, including other pathogens and media type, which have to date not been observed nor reported in a quantitative manner.

In LB, highly reactive 5-MCA cannot be detected during the exponential phase in any of the cell cultures (Fig. 3a–d). During intermediate growth stages, 5-MCA production increases corroborated by increasing current responses. The time points where 5-MCA is no longer detected differ between mono- and poly-microbial combination samples in LB. At later stages of growth, *Pa* no longer produces 5-MCA, likely due to a process leading to fast diminishment (e.g., reaction with oxygen). While there is an initial buildup of 5-MCA, current responses for this intermediate later decrease, which might be associated with factors in growth environments. Comparing polymicrobial samples in LB, the lowest 5-MCA current responses are observed in *Pa* and *Ec* sample (Fig. 3c). Similar to these results in LB, 5-MCA does not display redox peaks during the first 4 h of growth in TSB (Fig. 3e–h). Yet, once bacteria enter stationary growth phase, 5-MCA production rates increase in some cell cultures. In TSB-grown samples containing *Ec*, 5-MCA current responses are extremely small, particularly in the combinatorial sample containing all three pathogens (Fig. 3h). Furthermore, the SWV responses for 5-MCA differ based on media type, where in some cases 5-MCA amounts are higher in TSB compared to LB. Additionally, OHPHZ responses are significantly higher in various polymicrobial samples, specifically those with *Ec*, suggesting increased rates of PYO decomposition in these environmental conditions. Thus, these data illustrate that both the dynamics of polymicrobial co-cultures and media composition influence the rates of phenazine production.

To illustrate the dynamics of phenazine production between polymicrobial samples in two media, the ratios of peak currents of 5-MCA to PYO were plotted as a function of time (Fig. 5). Theoretically, assuming both metabolites have equal diffusion coefficients, the peak current ratio should be in proportion to the concentration ratio of 5-MCA to PYO. The 5-MCA/PYO current ratio is a significant parameter that reflects the standard rate constant of heterogeneous electron transfer (Dauphin-Ducharme et al., 2017; Mirceski et al., 2013). For *Pa* samples, 5-MCA to PYO peak current ratio is higher in TSB relative to LB, indicating that media components impact phenazine biosynthesis. Comparing co-culture samples in LB, 5-MCA to PYO current ratio is approximately two and one half times lower when *Pa* is co-cultured with

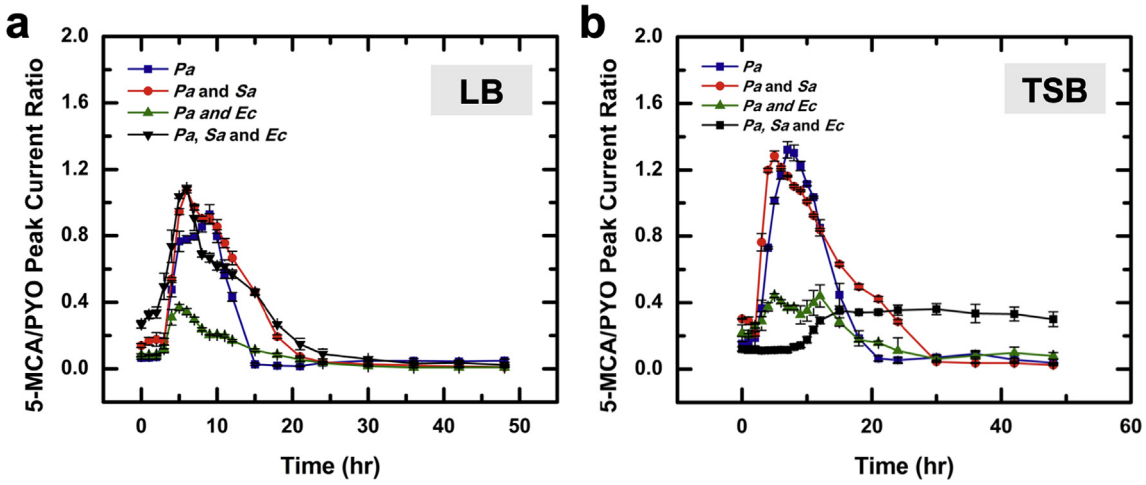

Fig. 5. Phenazine metabolites kinetics. 5-MCA/PYO peak currents ratios determined from *Pa* in different co-cultures in (a) LB and (b) TSB, shown as a function of time. Error bars plotted denote standard deviation between six samples.

Ec (Fig. 5a). On the other hand, polymicrobial samples in TSB display 5-MCA/PYO peak current ratios that are nearly three times lower in polymicrobial samples with *Ec* (Fig. 5b). Thus, variations in phenazine dynamics between polymicrobial samples in LB and TSB are observed, which contribute to different production rates (Fig. 4).

Using 5-MCA to PYO peak current ratios, the concentrations of 5-MCA were determined for mono- and poly-microbial samples in LB and TSB, which are summarized in Tables S3–S4 in the supplementary information. When grown individually, *Pa* produces a maximum 5-MCA concentration of 78 ± 5 μM and 220 ± 2 μM in LB and TSB (at 9 h), respectively. For polymicrobial combinations in LB, *Pa* produces the greatest 5-MCA concentration of 56 ± 3 μM in *Pa* and *Sa* (at 12 h), 9.9 ± 0.4 μM in *Pa* and *Ec* (at 11 h), and 12 ± 2 μM in *Pa*, *Sa* and *Ec* sample (at 11 h). When cultured with *Sa* in TSB, *Pa* produces 38 ± 2 μM as the highest 5-MCA concentration, at 21 h. For *Pa* co-cultured with *Ec* in TSB, the highest amount of 5-MCA was 2.8 ± 0.5 μM at 21 h. *Pa* produces 3.3 ± 0.9 μM as the maximum concentration of 5-MCA when all three pathogens were co-cultured together in TSB. The quantified 5-MCA concentrations were plotted as a function of growth time for two media (Fig. 4c and d). The maximum 5-MCA concentration in TSB is higher by a factor of 3 compared to LB for *Pa* samples. Yet, when cultured with *Sa*, *Pa* produces slightly higher amounts of 5-MCA in LB compared to TSB. The amounts of 5-MCA in *Pa* and *Sa* sample are marginally lower than in *Pa* culture, in LB. In contrast, 5-MCA concentrations in *Pa* and *Sa* co-culture are lower by a factor of 6 relative to the *Pa* monoculture in TSB. In both media, the presence of *Ec* results in more significant differences with notably small concentrations of 5-MCA produced.

We note that as a highly reactive intermediate (Bellin et al., 2014, 2016; Reyes et al., 1981; Simoska et al., 2019). 5-MCA might serve as a signaling molecule in redox balancing. The conversion of PCA to 5-MCA, and to PYO, involves additional functional groups derived from S-adenosylmethionine and molecular oxygen, respectively. The methylase PhzM is responsible for the conversion of PCA to 5-MCA. However, there is an unknown parameter that affects 5-MCA production, which needs to be examined in a future study. While 5-MCA production acts as a sink for PCA, a research study has shown that additional steps, requiring molecular oxygen, might have a significant influence on 5-MCA production (Xu et al., 2013). As a result, 5-MCA production might not directly correlate with available PCA. This observation further suggests that environmental factors may differentially regulate synthesis of this intermediate. Our distinct results in LB and TSB further illustrate the effect of environmental factors on 5-MCA concentrations produced in polymicrobial cultures. A recent study has shown that PYO production is activated only in the presence of NADH in addition to a required interaction between PhzM and PhzS enzymes (Parsons et al., 2007). *Pa* phenazine production is growth phase dependent as metabolites are produced in the stationary phase. During this stage, oxygen is limiting, resulting in NADH accumulation and an increased intercellular NADH/NAD^+ ratio (Price-Whelan et al., 2007), which is relieved by PYO redox balancing. Additionally, the growth conditions, such as nutrients, carbon and nitrogen sources, have significant effects on PYO production rates (Jayaseelan et al., 2014; Li et al., 2018; Simoska et al., 2019).

Fig. 4 shows distinct phenazine concentrations of PYO and 5-MCA in polymicrobial communities in each media. The presence of *Sa* in LB does not largely impact phenazine production, however, the concentrations of PYO and 5-MCA are lower by a factor of 2.5 and 4, respectively, in TSB. These results suggest that *Sa* and *Pa* compete for nutrients in TSB media, leaving far fewer nutrients available for *Pa*, which consequently decreases phenazine production. The presence of *Ec* in polymicrobial samples in each media significantly diminishes the rates of phenazine production. In particular, large differences are observed in polymicrobial co-cultures in TSB, where extremely small amounts of both PYO and 5-MCA are produced. A previous biological study has shown initial evidence of the ability of indole produced by *Ec* to quench PYO production and facilitate growth of *Ec* in mixed cultures (Chu et al., 2011). Produced as a signal molecule from the amino acid tryptophan by tryptophanase during stationary phase (J.-H. Lee and J. Lee, 2010; Pandey et al., 2019), indole inhibits cell division, thus allowing *Ec* to thrive over other bacteria in multispecies communities. Other research has suggested that indole has the capability to decrease virulence induced production in *Pa* by altering gene expression and interfering with quorum sensing mechanisms (J.-H. Lee and J. Lee, 2010). To test for indole presence in polymicrobial samples with *Ec*, Kovac's test was performed. This qualitative procedure, which determines bacteria's ability to produce indole by deamination of tryptophan, yielded a red-violet-pink top layer in cell cultures with *Ec* in each media at various growth times (6, 18, and 24 h), confirming the presence of indole in the polymicrobial combinations.

Although a previous study has shown the *Ec* can secrete indole concentrations up to 600 μM (J.-H. Lee and J. Lee, 2010), indole production might be critically affected by several environmental factors, such as cell population, carbon sources, pH, and temperature. Therefore, indole amounts produced likely diverge in different environmental conditions thus impacting phenazine production dynamics in various ways. These results highlight the importance of identifying environmental parameters that influence metabolism dynamics in diverse microbial communities, particularly in the context of polymicrobial infections. Phenazine production rates are likely regulated on multiple environmental levels, which have to be standardized with regard to

growth media to understand phenazine production dynamics.

3.5. Influence of growth media on phenazine production in polymicrobial environments

The quantitative results, shown in previous sections of this study, address how the relative phenazines production (Fig. 4) and ratio to other intermediates (Fig. 5) change during growth in response to various environmental factors. Most importantly changes in the dynamics are observed in the presence of other microbes, pH, and media composition. In this study, both LB and TSB liquid broths were used, which are rich with nutrients essential in supporting the growth of various microorganisms. Although there are many options when choosing growth media (e.g., phosphate buffered saline, buffered year extract broth, Mueller-Hinton broth, nutrient broth) (Li et al., 2018), these two complex media are the most predominant in studies with *Pa* reported in the literature (Table S5). In particular, LB and TSB contain different casein peptones, peptides, minerals, several vitamins and trace elements (e.g., S, Mg, N). Given their complexity and richness in nutrients, TSB and LB are reasonable choices of growth media herein. In prior research (Simoska et al., 2019), DESI-MS methods were employed to analyze differences in the composition of these media. Briefly, these results showed noteworthy distinctions between LB and TSB: (1) the relative abundance of choline (a water-soluble vitamin consumed by cells for production of toxins) at m/z 104.107 in the positive ion mode, and (2) the relative abundance of protonated and chlorinated hexose species (six-carbon sugars) at m/z 179.056 and m/z 215.032, respectively. Higher relative abundances for both choline and hexose species were detected in TSB relative to LB, which resulted in higher amounts of PYO produced in TSB for *Pa* monoculture (Simoska et al., 2019).

To better understand how components of each media might be contributing to observed variations in phenazine production, qualitative DESI-MS analyses were performed to compare relative abundances of choline and hexose species in polymicrobial combinations at 5 h growth. In the positive ion mode, the relative abundances of choline at m/z 104.107 for three different polymicrobial cultures in LB did not notably differ between samples (Fig. S1b), with the lowest abundance observed for the *Pa* and *Ec* sample (Figs. S1a and S2). Similarly, the relative abundances of this species were comparable between the three combination samples in TSB (Figs. S1a, S1c, S3). Higher relative abundances for choline were detected in samples in TSB compared to LB as depicted in the ion images in Fig. S1a. When *Pa* was cultured separately in LB or TSB, significantly lower abundances of choline were detected (Figs. S2b and S3b) in comparison to polymicrobial samples, suggesting high consumption of choline by individually grown *Pa*. Yet this is not observed in the polymicrobial samples, indicating that the presence of other pathogens changes choline consumption rates. In the negative ion mode, the relative abundances of hexose species did not considerably vary between three different polymicrobial combinations in LB and TSB (Figs. S4–S5). For *Pa* monocultures in TSB and LB, the hexose relative abundances are qualitatively higher compared to polymicrobial samples (Figs. S6–S7). Variation in the abundance of deprotonated and chlorinated hexose species are observed, likely due to possible changes occurring dependent on adduct type. These data suggest that pathogenic bacteria in these environments might compete for hexose and most likely numerous other nutrients in growth media. Consequently, growth media composition highly impacts phenazine production and dynamics in several ways as observed in our electrochemical results.

In addition to qualitatively comparing relative abundances of choline and hexose, DESI-MS analysis was performed to detect PYO and other cellular metabolites in polymicrobial samples in both growth media. Fig. 6 provides representative mass spectra and ion images (in the positive ion mode) for cellular PYO detected at m/z 211.086 in polymicrobial environments in LB and TSB. Higher relative abundances of PYO were observed in polymicrobial samples in LB than in TSB (Fig. 6a). A small decrease in PYO abundance was observed when all three pathogens were cultured together in LB (Fig. 6b). For polymicrobial combination tests in TSB, the highest PYO abundance was detected in *Pa* and *Sa* sample while the lowest PYO abundance was found in the sample containing all three bacterial types (Fig. 6c). Yet PYO was not detectable (S/N $<$ 3) in the mass spectra for *Pa* and *Ec* co-culture in TSB. These qualitative mass spectrometry results are in agreement with PYO trends in quantitative electrochemical data. In addition to PYO, other metabolites and enzymatic products from different polymicrobial cultures in each media were detected using DESI-MS (Figs. S4–S6). Multiple changes in metabolites abundances were observed: (1) succinate at m/z 117.019 was less abundant in *Pa* and *Sa* samples in LB and TSB, (2) disaccharide at m/z 377.085 was detected in lower abundances in polymicrobial samples with *Sa* present, and (3) abundances of citrate at m/z 191.019 and gluconate at m/z 195.051 were lower in samples containing *Ec*. As summarized in Fig. S6, metabolite distribution differs between growth media. While DESI-MS results provide useful information about media composition and additional cellular species produced in polymicrobial co-cultures, these results are only qualitative. Unlike our electrochemical method providing means for *in situ* quantitative analysis, DESI-MS measurements are associated with biases present in sampling times and sample drying effects, causing exposure to oxygen and cell death prior to analysis. Moreover, enhanced matrix and susceptibility to ion suppression associated with ambient ionization mass spectrometry methods lead to additional limitations for quantitative analysis of metabolites.

In these complex polymicrobial environments, bacteria might be feeding and competing for nutrients, and/or producing additional cellular metabolites dependent on the media type. Our results clearly demonstrate that in polymicrobial communities, the onset of infection changes drastically with respect to phenazine production rates. The presence of other bacteria significantly influences phenazine production in different ways, which is also heavily dependent on growth media. Our results call for the standardization for cell culture experiments, largely with respect to growth media components and quantities, as it is necessary to appropriately study the onset of polymicrobial infections. As summarized in Table S5, there are countless possibilities of growth media for culturing *Pa*, including nonstandard methods, such as synthetic cystic fibrosis sputum (Darch et al., 2018) and wound-like media (DeLeon et al., 2014). Yet, with standard growth media, such as LB and TSB, the real analytical concentrations of components likely vary between batches. Future research needs to focus on optimization, standardization, and certification of growth environment standards mainly because quantitative analytical chemistry is missing from standardization of assays. Specifically, it is necessary to understand particular media components and quantities to adequately assess which contribute to differences in phenazine dynamics. To understand how complex media influences development of infections, design of certified media standards that simulate environments for cystic fibrosis, biofilms and/or wound infections is essential, which is beyond the scope of this study. Therefore, the state of polymicrobial infections needs to be reexamined for biodiagnosis of *Pa* phenazine dynamics.

Our results, showing distinct dynamics of phenazine production with regard to growth in multispecies samples, point to the need for standard methods of growth media, which have great implications towards understanding the onset of bacterial infections, antibiotic resistance, and treatments. More extensive environmental factors need to be examined, however, our electrochemical approach provides the basis set as to the relative differences in phenazine production rates that can be quantified with high sensitivity. In follow-up work, the influence of additional factors (oxygen availability, host genetics, and antibiotics) on redox phenazine production will be monitored using T-CUAs.

4. Conclusions

In summary, this study shows quantitative electrochemical

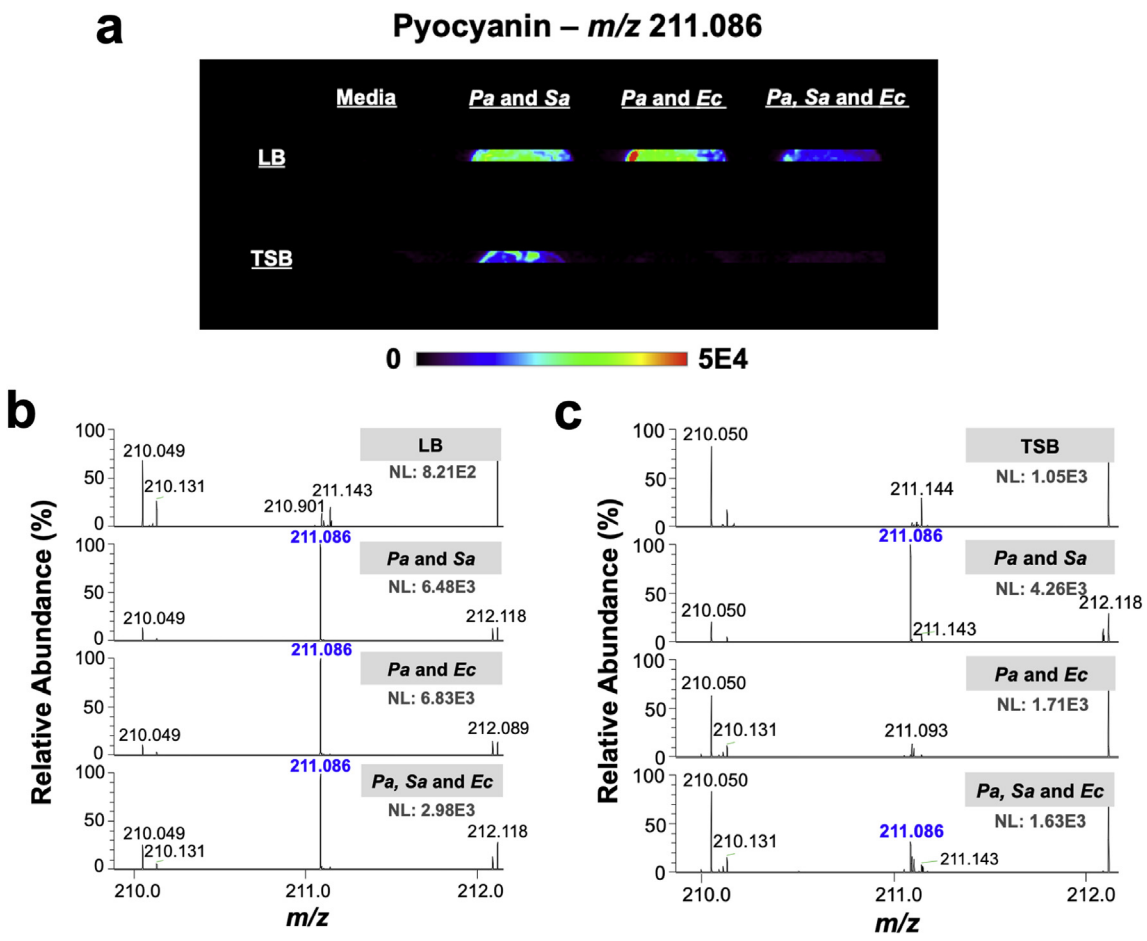

Fig. 6. DESI-MS data of PYO at *m/z* 211.086 obtained at 5 h of growth in different polymicrobial samples in LB and TSB. (a) DESI-MS ion images in *Pa* and *Sa*, *Pa* and *Ec*, and *Pa*, *Sa*, and *Ec* in each media. Relative abundances of PYO produced by *Pa* are higher in LB relative to TSB. Highest PYO relative abundances are observed in samples containing *Sa*. PYO relative abundances are lower in polymicrobial samples containing *Ec*, especially in TSB. These qualitative data are in agreement with electrochemical quantification of PYO. (b) DESI-MS spectra of PYO (positive ion mode) for polymicrobial samples in LB. (c) DESI-MS spectra of PYO (positive ion mode) for polymicrobial samples in TSB. PYO, secreted from *Pa*, is not detected in the DESI-MS spectra for LB and TSB only. NL represents ion abundance (ion current).

monitoring of the impact of polymicrobial communities on production rates of *Pa* phenazine metabolites in different growth media. Using T-CUAs as electrochemical sensors, the dynamics of phenazine biosynthesis were continually observed via detection of redox-active metabolites PYO, 5-MCA, OHPHZ, and an unknown species. These quantitative results demonstrate distinct electrochemical current responses for phenazines produced between *Pa* grown: (1) individually, and (2) in polymicrobial samples. In LB, the maximum concentrations of PYO were 150 ± 1 μM for *Pa*, 150 ± 1 μM for *Pa* and *Sa*, 72 ± 1 μM for *Pa* and *Ec*, and 28 ± 1 μM in *Pa*, *Sa* and *Ec* sample (at 21 h). In TSB, the highest PYO concentrations were 190 ± 5 μM for *Pa* (at 21 h), 78 ± 2 μM for *Pa* and *Sa* (at 21 h), 9.3 ± 0.2 μM for *Pa* and *Ec* (at 21 h), and 8.2 ± 0.5 μM in *Pa*, *Sa* and *Ec* sample (at 48 h). Additionally, the concentrations of highly reactive 5-MCA were determined. The presence of *Sa* caused a notable decrease in phenazine concentrations only in TSB while the presence of *Ec* in polymicrobial samples drastically quenched phenazine production rates in both media. These disparities likely correlate to (1) differences in nutrient consumption, and (2) other cellular metabolites produced, in polymicrobial environments. These results clearly demonstrate that presence of other bacteria dramatically impacts phenazine production rates, which also directly depends on the media type. The media type strongly influences phenazine product distribution, especially in polymicrobial co-cultures. Therefore, these data imply the need for analytical standardization of simulation media, which represent key attributes of *in vivo* environments (e.g., wounds, cystic fibrosis lungs). Our T-CUAs electroanalytical method has the sensitivity to distinguish differences based on correlative measurements in media not only on phenazine production but also on intermediates produced in polymicrobial samples. Thus, these data support use of T-CUAs in biodiagnosis and monitoring of *Pa* infections colonized by multiple bacteria.

Future work will focus on electrochemical monitoring of *Pa* phenazine production in the presence of other relevant pathogens, such as *Enterococcus faecalis* and *Staphylococcus epidermidis*, as well as in the presence of eukaryotic, host cells (e.g., macrophages). Moreover, studies need to be performed with additional, increased co-cultures comprising of more than three pathogens. Additionally, phenazine production and dynamics need to be examined on T-CUAs with clinically relevant *Pa* strains isolated from patients, as clinical strains grow at different rates dependent on environmental conditions and composition (Wu et al., 2019). Finally, the state of infection in these polymicrobial populations needs to be reexamined for diagnosis, specifically with respect to standardization of simulated growth media.

Author contributions

O.S. performed electrode fabrication, all electrochemical measurements, data analysis and characterization. O.S. prepared cell cultures and took OD600 measurements. O.S. and M.S. performed MS

experiments. M.S. performed DESI-MS imaging analysis. O.S. and K.J.S. designed studies, planned experiments, analyzed data and wrote the manuscript. All authors contributed to editing the paper.

CRediT authorship contribution statement

Olja Simoska: Conceptualization, Data curation, Formal analysis, Investigation, Methodology, Writing - original draft. **Marta Sans:** Formal analysis, Writing - review & editing, Writing - original draft. **Livia S. Eberlin:** Formal analysis, Writing - review & editing, Writing - original draft. **Jason B. Shear:** Writing - review & editing. **Keith J. Stevenson:** Conceptualization, Formal analysis, Supervision, Writing - review & editing, Writing - original draft.

Acknowledgements

O.S. acknowledges the support from an ACS Division of Analytical Chemistry Graduate Fellowship sponsored by the Society of Analytical Chemists of Pittsburgh (SACP) and the S.R.F.A career development grant. Financial support for this work was provided by the Welch Foundation (grants F-1529 (to K.J.S.) and F-1331 (to J.B.S)) and the K.J.S and S.L. lifetime achievement fund.

Appendix A. Supplementary data

Supplementary data to this article can be found online at https://doi.org/10.1016/j.bios.2019.111538.

References

Alatraktchi, F., Breum Andersen, S., Krogh Johansen, H., Molin, S., Svendsen, W., 2016a. Sensors 16, 408–418.
Alatraktchi, F.A., Johansen, H.K., Molin, S., Svendsen, W.E., 2016b. Nanomedicine 11, 2185–2195.
Alatraktchi, F.A., Noori, J.S., Tanev, G.P., Mortensen, J., Dimaki, M., Johansen, H.K., Madsen, J., Molin, S., Svendsen, W.E., 2018. PLoS One 13 e0194157– e0194159.
Alves, P.M., Al-Badi, E., Withycombe, C., Jones, P.M., Purdy, K.J., Maddocks, S.E., 2018. Pathog. Dis. 76, 67–77.
Atkinson, S., Williams, P., 2009. J. R. Soc. Interface 6, 959–978.
Bassler, B.L., Losick, R., 2006. Cell 125, 237–246.
Bellin, D.L., Sakhtah, H., Rosenstein, J.K., Levine, P.M., Thimot, J., Emmett, K., Dietrich, L.E.P., Shepard, K.L., 2014. Nat. Commun. 5, 3256–3266.
Bellin, D.L., Sakhtah, H., Zhang, Y., Price-Whelan, A., Dietrich, L.E.P., Shepard, K.L., 2016. Nat. Commun. 7, 10535–10545.
Bergeron, A.C., Seman, B.G., Hammond, J.H., Archambault, L.S., Hogan, D.A., Wheeler, R.T., 2017. Infect. Immun. 85 e00475-17.
Bertesteanu, S., Triaridis, S., Stankovic, M., Lazar, V., Chifiriuc, M.C., Vlad, M., Grigore, R., 2014. Int. J. Pharm. 463, 119–126.
Bosire, E.M., Rosenbaum, M.A., 2017. Front. Microbiol. 8, 5026–5037.
Boucher, H.W., Talbot, G.H., Bradley, J.S., Edwards, J.E., Gilbert, D., Rice, L.B., Scheld, M., Spellberg, B., Bartlett, J., 2009. Clin. Infect. Dis. 48, 1–12.
Bowler, P.G., Duerden, B.I., Armstrong, D.G., 2001. Clin. Microbiol. Rev. 14, 244–269.
Buzid, A., Shang, F., Reen, F.J., Muimhneacháin, E.Ó., Clarke, S.L., Zhou, L., Luong, J.H.T., O'Gara, F., McGlacken, G.P., Glennon, J.D., 2016. Sci. Rep. 6, 30001–30009.
Chu, W., Zere, T.R., Weber, M.M., Wood, T.K., Whiteley, M., Hidalgo-Romano, B., Valenzuela Jr., E., McLean, R.J.C., 2011. Appl. Environ. Microbiol. 78, 411–419.
Connell, J.L., Ritschdorff, E.T., Whiteley, M., Shear, J.B., 2013. Proc. Natl. Acad. Sci. U.S.A. 110, 18380–18385.
Culotti, A., Packman, A.I., 2014. PLoS One 9 e107186–9.
Darch, S.E., Simoska, O., Fitzpatrick, M., Barraza, J.P., Stevenson, K.J., Bonnecaze, R.T., Shear, J.B., Whiteley, M., 2018. Proc. Natl. Acad. Sci. U.S.A. 5, 4779–4784.
Dauphin-Ducharme, P., Arroyo-Currás, N., Kurnik, M., Ortega, G., Li, H., Plaxco, K.W., 2017. Langmuir 33, 4407–4413.
DeLeon, S., Clinton, A., Fowler, H., Everett, J., Horswill, A.R., Rumbaugh, K.P., 2014. Infect. Immun. 82, 4718–4728.
Diederich, C., Leypold, M., Culka, M., Weber, H.X.R., Breinbauer, R., Ullmann, G.M., Blankenfeldt, W., 2017. Sci. Rep. 1–13.
Dietrich, L.E.P., Price-Whelan, A., Petersen, A., Whiteley, M., Newman, D.K., 2006. Mol. Microbiol. 61, 1308–1321.
Duay, J., Elliott, J., Shear, J.B., Stevenson, K.J., 2015. Anal. Chem. 87, 10109–10116.
Duay, J., Goran, J.M., Stevenson, K.J., 2014. Anal. Chem. 86, 11528–11532.
Elliott, J., Duay, J., Simoska, O., Shear, J.B., Stevenson, K.J., 2017a. Anal. Chem. 89, 1267–1274.
Elliott, J., Simoska, O., Karasik, S., Shear, J.B., Stevenson, K.J., 2017b. Anal. Chem. 89, 6285–6289.
Fetzer, A.F., Werner, A.S., Hagstrom, J.W., 1967. Am. Rev. Respir. Dis. 96, 1121–1130.
Fick, R.B., 1989. Chest 96, 158–164.
Gandouzi, I., Tertis, M., Cernat, A., Saidane-Mosbahi, D., Ilea, A., Cristea, C., 2019. Materials 12, 1180–1193.
Giacometti, A., Cirioni, O., Schimizzi, A.M., Del Prete, M.S., Barchiesi, F., D'Errico, M.M., Petrelli, E., Scalise, G., 2000. J. Clin. Microbiol. 38, 918–922.
Glasser, N.R., Kern, S.E., Newman, D.K., 2014. Mol. Microbiol. 92, 399–412.
Goluch, E.D., 2017. Trends Biotechnol. 35, 1125–1128.
Hendiani, S., Pornour, M., Kashef, N., 2019. Photodiagn. Photodyn. Ther. 1–18.
Henke, J.M., Bassler, B.L., 2004. Trends Cell Biol. 14, 648–656.
Jayaseelan, S., Ramaswamy, D., Dharmaraj, S., 2014. World J. Microbiol. Biotechnol. 30, 1159–1168.
Jayaseelan, S., Ramaswamy, D., Dharmaraj, S., 2013. World J. Microbiol. Biotechnol. 30, 1159–1168.
Klevens, R.M., Edwards, J.R., Richards, C.L., Horan, T.C., Gaynes, R.P., Pollock, D.A., Cardo, D.M., 2007. Public Health Rep. 122, 160–166.
Korgaonkar, A., Trivedi, U., Rumbaugh, K.P., Whiteley, M., 2013. Proc. Natl. Acad. Sci. U.S.A. 110, 1059–1064.
Lee, D.-H., Koh, E.-H., Choi, S.-R., Kim, S., 2013. Ann. Lab. Med. 33 406–4.
Lee, J.-H., Lee, J., 2010. FEMS Microbiol. Rev. 34, 426–444.
Li, S., Mou, Q., Feng, N., Leung, P.H.M., 2018. Int. J. Electrochem. Sci. 13, 3789–3798.
Llor, C., Bjerrum, L., 2014. Ther. Adv. Drug Saf. 5, 229–241.
Magill, S.S., Edwards, J.R., Bamberg, W., Beldavs, Z.G., Dumyati, G., Kainer, M.A., Lynfield, R., Maloney, M., McAllister-Hollod, L., Nadle, J., Ray, S.M., Thompson, D.L., Wilson, L.E., Fridkin, S.K., 2014. N. Engl. J. Med. 370, 1198–1208.
Mavrodi, D.V., Blankenfeldt, W., Thomashow, L.S., 2006. Annu. Rev. Phytopathol. 417–445.
Mavrodi, D.V., Bonsall, R.F., Delaney, S.M., Soule, M.J., Phillips, G., Thomashow, L.S., 2001. J. Bacteriol. 183, 6454–6465.
Mavrodi, D.V., Peever, T.L., Mavrodi, O.V., Parejko, J.A., Raaijmakers, J.M., Lemanceau, P., Mazurier, S., Heide, L., Blankenfeldt, W., Weller, D.M., Thomashow, L.S., 2010. Appl. Environ. Microbiol. 76, 866–879.
Mirani, Z.A., Fatima, A., Urooj, S., Aziz, M., Khan, M.N., Abbas, T., 2018. Iran J. Basic Sci. Med. 21, 760–770.
Mirceski, V., Laborda, E., Guziejewski, D., Compton, R.G., 2013. Anal. Chem. 85, 5586–5594.
Noto, M.J., Burns, W.J., Beavers, W.N., Skaar, E.P., 2017. J. Bacteriol. 199 616–13.
O'Brien, S., Fothergill, J.L., 2017. FEMS Microbiol. Lett. 364, 850.
Pandey, R., Swamy, K.V., Khetmalas, M.B., 2019. IJBT 12, 297–310.
Parsons, J.F., Greenhagen, B.T., Shi, K., Calabrese, K., Robinson, H., Ladner, J.E., 2007. Biochemistry 46, 1821–1828.
Pierson, L.S., Pierson, E.A., 2010. Appl. Microbiol. Biotechnol. 86, 1659–1670.
Price-Whelan, A., Dietrich, L.E.P., Newman, D.K., 2007. J. Bacteriol. 189, 6372–6381.
Reyes, E.A.P., Bale, M.J., Cannon, W.H., Matsen, J.M., 1981. J. Clin. Microbiol. 13, 456–458.
Ringen, L.M., Drake, C.H., 1952. J. Bacteriol. 64, 841–845.
Rohmer, L., Hocquet, D., Miller, S.I., 2011. Trends Microbiol. 19, 341–348.
Santiveri, C.R., Sismaet, H.J., Kimani, M., Goluch, E.D., 2018. Chemistry 3, 2926–2930.
Schiessl, K.T., Hu, F., Jo, J., Nazia, S.Z., Wang, B., Price-Whelan, A., Min, W., Dietrich, L.E.P., 2019. Nat. Commun. 10, 762–772.
Shah, A., Ullah, A., Nosheen, E., Rana, U.A., Shakir, I., Badshah, A., Rehman, Z.U., Hussain, H., 2013. J. Electrochem. Soc. 160, H765–H769.
Sharp, D., Gladstone, P., Smith, R.B., Forsythe, S., Davis, J., 2010. Bioelectrochemistry 77, 114–119.
Simoska, O., Sans, M., Fitzpatrick, M.D., Crittenden, C.M., Eberlin, L.S., Shear, J.B., Stevenson, K.J., 2019. ACS Sens. 4, 170–179.
Sismaet, H.J., Pinto, A.J., Goluch, E.D., 2017. Biosens. Bioelectron. 97, 65–69.
Stevens, A.M., Schuster, M., Rumbaugh, K.P., 2012. J. Bacteriol. 194, 2131–2141.
Sullivan, N.L., Tzeranis, D.S., Wang, Y., So, P.T.C., Newman, D., 2011. ACS Chem. Biol. 6, 893–899.
Walker, T.S., 2004. Plant Physiol. 134, 320–331.
Webster, T.A., Goluch, E.D., 2012. Lab Chip 12, 5195–5201.
Webster, T.A., Sismaet, H.J., Conte, J.L., Chan, I.-P.J., Goluch, E.D., 2014. Biosens. Bioelectron. 60, 265–270.
Wu, X., Siehnel, R.J., Garudathri, J., Staudinger, B.J., Hisert, K.B., Ozer, E.A., Hauser, A.R., Eng, J.K., Manoil, C., Singh, P.K., Bruce, J.E., 2019. J. Proteome Res. 18, 2601–2612.
Xu, N., Ahuja, E.G., Janning, P., Mavrodi, D.V., Thomashow, L.S., Blankenfeldt, W., 2013. Acta Crystallogr. Sect. D Biol. Crystallogr. 69, 1403–1413.
Zheng, H., Kim, J., Liew, M., Yan, J.K., Herrera, O., Bok, J.W., Kelleher, N.L., Keller, N.P., Wang, Y., 2015. Curr. Biol. 25, 29–37.